AFRL-MN-EG-TR-2001-7091

MODELING AND ANALYSIS OF REACTIVE COMPACTION FOR GRANULAR ENERGETIC SOLIDS

Keith A. Gonthier
Mechanical Engineering Department
Louisiana State University
Baton Rouge, LA 70803

SEPTEMBER 2001

FINAL REPORT FOR PERIOD MAY 2001 – AUGUST 2001

DISTRIBUTION A: Approved for public release; distribution unlimited

AIR FORCE RESEARCH LABORATORY, MUNITIONS DIRECTORATE
Air Force Materiel Command ■ United States Air Force ■ Eglin Air Force Base

20011005 187

NOTICE

When Government drawings, specifications, or other data are used for any purpose other than in connection with a definitely Government-related procurement, the United States Government incurs no responsibility or any obligation whatsoever. The fact that the Government may have formulated or in any way supplied the said drawings, specifications, or other data, is not to be regarded by implication, or otherwise in any manner construed, as licensing the holder, or any other person or corporation; or as conveying any rights or permission to manufacture, use, or sell any patented invention that may in any way be related thereto.
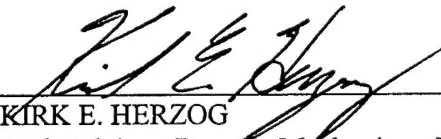
This technical report is releasable to the National Technical Information Services (NTIS). At NTIS it will be available to the general public, including foreign nations.

This technical report has been reviewed and is approved for publication.

FOR THE COMMANDER

PAUL K. LAIRD
Tech Director, Ordnance Division

KEITH M. ROESSIG, Capt, USAF
Program Manager

KIRK E. HERZOG
Tech Advisor, Damage Mechanisms Branch

Anyone having need for a copy of this report should first contact the Defense Technical Information Center (DTIC) at the address shown below. If you are a registered DTIC User, DTIC can provide you with a copy. Please do not request copies from the Air Force Research Laboratory, Munitions Directorate. Requests for additional copies should be directed to:

> Defense Technical Information Center (DTIC)
> 8725 John J. Kingman Road, Ste 0944
> Ft Belvoir, VA 22060-6218

This report is published in the interest of the scientific and technical information exchange. Publication of this report does not constitute approval or disapproval of the ideas or findings

If your address has changed, if you wish to be removed from our mailing list, or if your organization no longer employs the addressee, please notify AFRL/MNMW, Eglin AFB FL 32542-6810, to help us maintain a current mailing list. Do not return copies of this report unless contractual obligations or notice on a specific document requires that it be returned.

REPORT DOCUMENTATION PAGE

1. AGENCY USE ONLY *(Leave blank)*	2. REPORT DATE 2001 SEPTEMBER	3. REPORT TYPE AND DATES COVERED FINAL MAY 2001 – AUGUST 2001

4. TITLE AND SUBTITLE MODELING AND ANALYSIS OF REACTIVE COMPACTION FOR GRANULAR ENERGETIC SOLIDS	5. FUNDING NUMBERS JON:25020693 PE:62602F PR:2502 TA:06 WU:93
6. AUTHOR(S) DR. KEITH A. GONTHIER	

7. PERFORMING ORGANIZATION NAME(S) AND ADDRESS(ES) PROGRAM MANAGER: CAPT KEITH M. ROESSIG (850) 882-9643 EXT. 266 Mechanical Engineering Department Louisiana State University Baton Rouge, LA 70803 AFRL/MNMW 101 W. EGLIN BLVD. STE 135 EGLIN AFB, FL 32542-6810	8. PERFORMING ORGANIZATION REPORT NUMBER AFRL-MN-EG-TR-2001-7091

9. SPONSORING/MONITORING AGENCY NAME(S) AND ADDRESS(ES) Associate Programs - TJ 2114 National Research Council 2101 Constitution Avenue NW Washington, DC 20418	10. SPONSORING/MONITORING AGENCY REPORT NUMBER

11. SUPPLEMENTARY NOTES
 The work presented here was completed at the Advanced Warhead Experimentation Facility (Site C64-C) of the Damage Mechanisms Branch of the AFRL Munitions Directorate. Funding and sponsorship provided through the Summer Faculty Fellowship Program under the National Research Council and the Air Force Office of Scientific Research.

12a. DISTRIBUTION/AVAILABILITY STATEMENT DISTRIBUTION A: Approved for public release; distribution unlimited	12b. DISTRIBUTION CODE (Leave this block blank)

13. ABSTRACT:

A technique is described for modeling mechanically induced localized heating and ignition at the grain scale (meso-scale) of granular reactive solids that maintains proper consistency with the experimentally characterized bulk (macro-scale) material behavior. The technique is illustrated for the dynamic compaction, localized heating, and ignition of granular HMX due to mild impact of a constant speed piston (~86 m/s). Guided by basic principles of contact mechanics, bulk dissipated mechanical energy is thermalized at localization sites (hot-spots) within the material meso-structure which are centered at intergranular contact points (surfaces). The evolution of bulk quantities is tracked at the macro-scale and the evolution of hot-spot temperature, mass fraction, and reaction progress are tracked at the meso-scale. Model predictions indicate that the onset of sustained combustion occurs for a piston speed that agrees well with confined Deflagration-to-Detonation Transition (DDT) experiments. This result suggests that the coupling technique may provide a rational framework for the development of improved energy localization, and ignition models for heterogeneous reactive solids. Results of a parametric sensitivity analysis show that the model is reasonably insensitive to variation in key energy localization parameters.

14. SUBJECT TERM Mechanical ignition; reactive flow; shock wave; equation of state; detonation velocity; grain size distribution	15. NUMBER OF PAGES 19
	16. PRICE CODE

17. SECURITY CLASSIFICATION OF REPORT UNCLASSIFIED	18. SECURITY CLASSIFICATION OF THIS PAGE UNCLASSIFIED	19. SECURITY CLASSIFICATION OF ABSTRACT UNCLASSIFIED	20. LIMITATION OF ABSTRACT UL

Contents

List of Figures

List of Tables

1 Introduction

It is well established that thermal energy localization resulting from the rapid deformation of heterogeneous reactive solids, such as propellants, pyrotechnics, and high-explosives, is important in the ignition and onset of sustained combustion in these materials. Mechanically induced ignition and combustion are particularly relevant to defense related applications requiring the safe handling and storage of reactive solids and the development of modern insensitive munitions. Localization typically occurs at the scale of heterogeneity (i.e., meso-scale or grain scale) due to various processes including inelastic grain and binder deformation, intergranular friction, and grain fracture. Importantly, energy localization at the meso-scale can have a significant effect on the large scale (macro-scale) material response, possibly triggering detonation [16].

Mathematical modeling can be used to better understand the interplay of localized heating and ignition at the meso-scale and the bulk system response at the macro-scale. Such modeling necessarily involves the coupling of physical phenomena occurring over disparate length and time scales. Several bulk models have been developed that describe mechanically induced transition to detonation for both pressed and granular explosives [1, 12, 15]. Often these models are only predictive over a narrow range of impact conditions. This deficiency is largely due to inaccurate descriptions of meso-scale phenomena, such as energy localization and ignition, also referred to as hot-spot formation, within the context of the bulk models. Some models give a more complete description than others. The Baer and Nunziato [1] model does not explicitly account for hot-spot formation but specifies an ignition criterion that is based solely on bulk quantities. The model of Johnson, et al [12], does account for hot-spot formation, though it imposes a constant value for hot-spot mass fraction, rather than describing its evolution, and estimates hot-spot temperature based on the bulk shock pressure. A more complete description is given by the model of Massoni, et al [15]. Their composite model tracks the evolution of hot-spot temperature and mass fraction by viscoplastic pore collapse, in a manner similar to that first proposed by Kang, et al [14], and couples this hot-spot model with a bulk, two-phase mixture model. However, due to the complexity of their composite model, it is unlikely that the energetics described by the hot-spot and two-phase models are consistent. Other models have been developed that track growth and decay of hot-spots to predict explosion times and thresholds based on imposed initial conditions for hot-spot size and temperature [3, 7, 23].

The main goal of this study is to develop and explore a technique for formulating a comprehensive and predictive model of mechanically induced hot-spot formation and ignition in heterogeneous reactive solids. The technique requires 1) a model for the bulk material response, 2) a model for the meso-scale structure (e.g., grain size, grain packing, etc.), 3) a localization strategy for depositing bulk dissipated mechanical energy at the meso-scale, and 4) a model for the meso-scale response. The meso-scale response will allow for the evolution of hot-spot temperature and mass fraction, subject to the localization strategy, rather than imposing their values. Here, it is assumed that the bulk material response is experimentally well-characterized and is accurately predicted by the bulk model; as such, we will maintain the integrity of bulk model predictions and require that the integrated mass, momentum, and energy of the meso-scale model locally equals that given by the bulk model. Moreover, this constraint is consistent with the common interpretation that the bulk response is an average manifestation of the meso-scale response. Models that do not explicitly enforce this constraint may give inconsistent meso-scale and bulk predictions. While such a constraint may be overly restrictive, it does provide a rational framework from which to formulate and explore the implications of various localization strategies.

1

In this study, some rigor is sacrificed in favor of tractability. Rather than considering a heterogeneous system of explosive grains embedded within a plastic-like binder (e.g., PBXs), we focus only on the explosive grains. The response of granular explosives to dynamic loading is of interests as they are typically the main load bearing constituent of PBXs. In particular, we model the dynamic compaction of granular HMX (cyclo-tetramethylene-tetranitramine) because it is both commonly used in aerospace and defense related applications and its quasi-static compaction behavior is experimentally well-characterized [5]. Further, the dynamic compaction and Deflagration-to-Detonation Transition (DDT) of granular HMX have been extensively studied [1, 2, 4, 9, 16, 18, 21]. Experimental data indicate that sustained combustion and DDT of confined granular HMX can be readily triggered by compaction waves resulting from weak mechanical impact (piston speeds $\sim 80-90$ m/s) [16, 22]; thus, a fairly well-defined threshold exists for comparing our model predictions against. Other modeling simplifications made in this study are discussed in appropriate sections of this report. Though this study focuses only on granular HMX, the technique can be generalized and applied to systems containing a binder phase as the physical, modeling, and computational issues involved are similar.

An outline of this report is as follows. First, a brief discussion of dynamic compaction is given and key issues related to thermal energy localization and ignition are identified. Second, the mathematical model is posed and the localization strategy explained. Third, the model is numerically solved to give predictions for localized heating and ignition of granular HMX. The piston speed needed to induce sustained combustion is predicted and compared to experiments, the sensitivity of the model to variations in key localization parameters is demonstrated, and the influence of grain size on the predicted threshold for sustained combustion is determined. Lastly, some conclusions and suggestions for future work are given.

2   Dynamic Compaction

A common paradigm for the dynamic compaction of a granular material is the piston impact problem shown in Fig. 1(a). In the figure, the uncompacted material has 30% porosity ($\phi_0 = 0.70$) and is in an unstressed state; this initial porosity is representative of loose granular energetic solids. Compaction is induced by a piston moving with constant speed ($U_p = 100$ m/s). Upon piston impact, compaction energy is transmitted through the material by shear and compression waves that involve interactions between grains through their contact surfaces, as illustrated in Fig. 1(b). These local grain interactions result in both stress and temperature fluctuations within the material meso-scale structure. The integrated effect of these fluctuations gives rise to a bulk wave that propagates away from the piston ($D \approx 400$ m/s) leaving the material in a stressed, compacted state with low porosity ($\phi_c \approx 0.96$); this wave is commonly referred to as a dynamic compaction wave. The compaction process is not instantaneous, but occurs over a finite length zone ($d \approx 4$ mm) referred to as the compaction zone. Within the compaction zone, the granular material is rapidly deformed and heated due to dissipative interactions between grains; common heating mechanisms include intergranular friction, grain fracture, plastic deformation of grains, and compression of grains. Temperature fluctuations within the compaction zone can be significant. If the deformation rates are sufficiently high, these dissipative processes will lead to the formation of thin, localized regions of intense heating near the contact surfaces between grains as there is little time for thermal cooling by conduction into the cooler grain interiors. For example, using the values depicted in Fig. 1, the bulk strain rate of the granular material induced by the compaction wave is approximately given by $\dot{\epsilon} = (1 - \phi_0/\phi_c)/\mathcal{T} = 0.203$ μs^{-1}, where $\mathcal{T} = d/(D - U_p) = 13.3$ μs is the residence time of a grain within the compaction zone. It will be shown in Section 4 that such strain
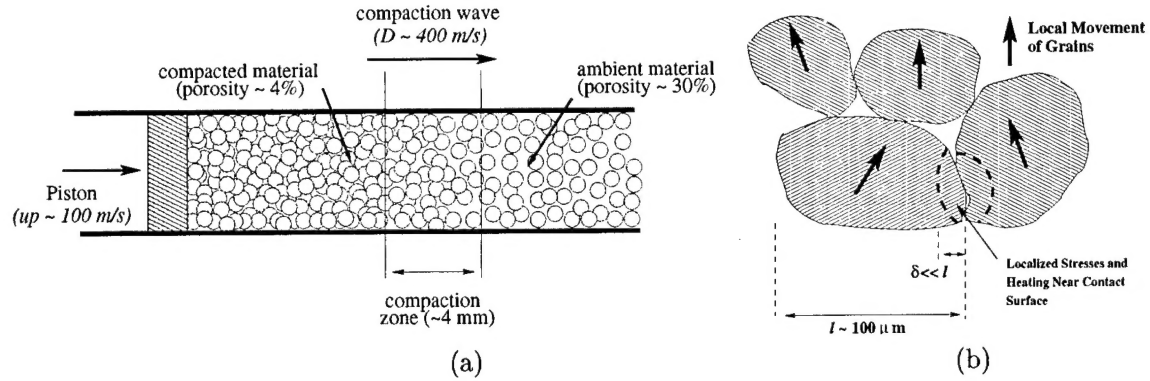
2

Figure 1: Schematic of a dynamic compaction process: (a) propagation of a bulk compaction wave; (b) localized stresses and grain heating at the contact surface between grains.

rates can result in significant volumetric heating rates in the vicinity of intergranular contact points (e.g., 5.0×10^5 GW/m^3). Using the thermal diffusivity of solid HMX, $\alpha = 1.76 \times 10^{-7}$ m^2/s, and assuming that all heating occurs at intergranular contact surfaces, the distance that thermal energy is conducted into a grain within the compaction zone, identified by δ in Fig. 1(b), is approximately $\delta = \sqrt{\alpha/\mathcal{T}} = 1.5$ μm $\ll l$, where $l \approx 100$ μm is an average grain size. Consequently, for the case shown here, thermal energy will be localized near grain contact surfaces within the compaction zone. The existence of these fine-scale features poses significant modeling and computational challenges that will be described later in this report. Compaction induced thermal energy localization in energetic solids can be a major mechanism for combustion initiation. If a sufficiently large number of intense localization sites exist, prompt initiation of sustained combustion will result and explosion is possible.

3 Mathematical Model

A mathematical model for compaction induced hot-spot formation is outlined in this section. The bulk compaction model is first given followed by the meso-scale energy localization model. Throughout this section, specific functional dependencies of some variables are emphasized to highlight the coupling of the bulk and meso-scale models.

3.1 Bulk Compaction Model

A one-dimensional (1-D) bulk compaction model is used in this study. Though there can exist substantial stress bridging between grains at the meso-scale [17, 20], resulting in spatially 3-D flow, the spatially averaged response can be approximated as 1-D provided that appropriate boundary conditions are specified. Stress bridging is, however, an important issue concerning energy localization that will be discussed later. The bulk compaction model was formulated by Gonthier et al [9]; as such, the reader is referred there for details. Here, we briefly summarize the bulk model, focusing on issues relevant to compaction induced localized heating.

3

The bulk model equations are given by

$$\frac{\partial}{\partial t}\begin{pmatrix} \rho \\ \rho u \\ \rho E \end{pmatrix} + \frac{\partial}{\partial x}\begin{pmatrix} \rho u \\ \rho u^2 + P \\ \rho u\left(E + P/\rho\right) \end{pmatrix} = \vec{0},$$ (1)

$$\frac{\partial \phi}{\partial t} + u\frac{\partial \phi}{\partial x} = \frac{\phi\left(1-\phi\right)}{\mu_c}\left(P_s - \beta\right),$$ (2)

$$\frac{\partial \tilde{\phi}}{\partial t} + u\frac{\partial \tilde{\phi}}{\partial x} = \begin{cases} \frac{1}{\tilde{\mu}}\left(f - \tilde{\phi}\right) & \text{if } f > \tilde{\phi}, \\ 0 & \text{otherwise.} \end{cases}$$ (3)

Independent variables these equations are time t and position x. Dependent variables for the granular solid are density ρ; velocity u; pressure P; total mass specific energy $E = e + u^2/2$, where e is the mass specific internal energy; solid volume fraction ϕ; no-load volume fraction $\tilde{\phi}$; intragranular stress $\beta(\phi, \tilde{\phi})$; and equilibrium no-load volume fraction $f(\phi)$. Quantities associated with the pure phase solid, denoted by subscript "s", are related to the granular solid variables by $\rho_s = \rho/\phi$, $P_s = P/\phi$, and $e_s = e - B$, where $B(\phi - \tilde{\phi}) = \int_0^{\phi'}\frac{\beta}{\rho}d\phi'$ is recoverable compaction energy. The parameters μ_c and $\tilde{\mu}$ appearing in Eqs. (2) and (3) govern the rates of relaxation to the equilibria $P_s = \beta$ and $f = \tilde{\phi}$, respectively. The system of equations is mathematically closed given equations of state $P_s(\rho_s, T)$ and $e_s(\rho_s, T)$, where T is the bulk temperature of the granular solid. In this study, we slightly modify the inert compaction model of Ref. [9] to account for chemical reaction and take $e_s(T, \lambda) = c_v T - \lambda q$, assuming an incompressible solid, where c_v is the specific heat at constant volume, λ is a bulk reaction progress variable that is determined by the meso-scale response, and q is the specific heat of reaction; the inclusion of chemical reaction is further explained in the following section.

Equation (1) is a system of conservation expressions for the granular solid mass, momentum, and total energy. Equations (2) and (3) are evolution equations for ϕ and $\tilde{\phi}$, constructed so that irreversible compaction is compatible with the Second Law of Thermodynamics. It is noted that for an incompressible solid, the mechanical response of the granular material, given by the mass and momentum expressions of Eq. (1), and Eqs. (2) and (3), is independent of the thermal response. This note will prove useful later.

We focus on compaction energetics which is important for the development of the energy localization model. Because low pressure compaction (< 100 MPa) associated with weak initiation of DDT induces only small density changes, we assume an incompressible solid and ignore compression work. In this case, it can be shown from Eqs. (1-3) that the evolution of internal energy for the granular material is given by

$$\frac{de}{dt} = \frac{de_s}{dt} + \frac{dB}{dt},$$ (4)

where

$$\frac{de_s}{dt} = \frac{\left(P_s - \beta\right)}{\rho}\frac{d\phi}{dt} + \frac{\beta}{\rho}\frac{d\tilde{\phi}}{dt},$$ (5)

$$\frac{dB}{dt} = \frac{\beta}{\rho}\frac{d}{dt}\left(\phi - \tilde{\phi}\right).$$ (6)

Here, $d/dt = \partial/\partial t + u\partial/\partial x$ is the convective derivative. Equations (5) and (6) describe the evolution of bulk thermal energy and recoverable compaction energy, respectively. We are particularly
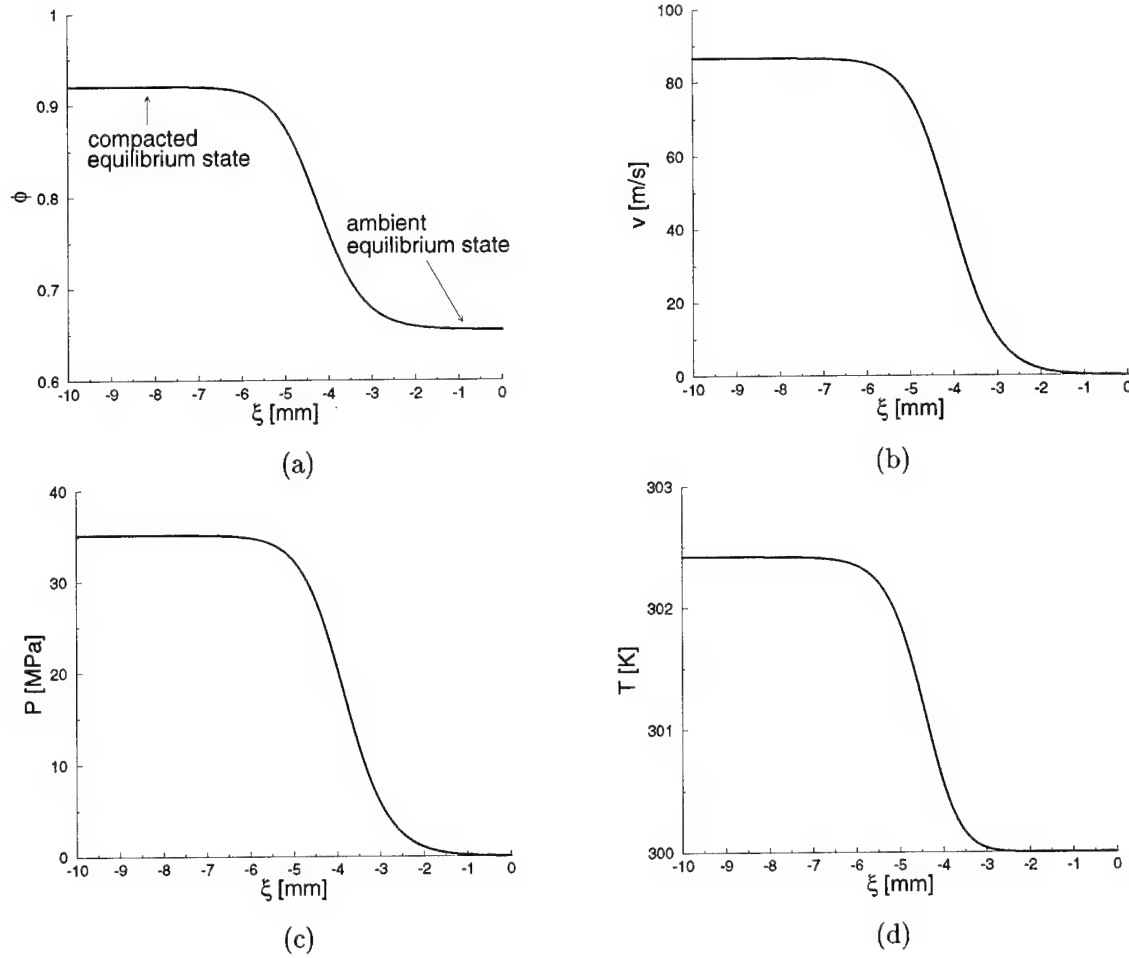
4

Figure 2: Predicted variation in bulk properties through the compaction zone for the inert compaction of granular HMX by a $u_p = 85.6$ m/s piston: (a) solid volume fraction, (b) velocity, (c) pressure, and (d) temperature.

interested in Eq. (5) as bulk thermal energy will be deposited at the meso-scale based on our localization strategy. Entropy considerations indicate that each term on the right side of Eq. (5) is dissipative.

To illustrate features of the bulk compaction model, representative predictions for the spatial variation in the bulk quantities ϕ, u, P_s, and T through the compaction zone of an inert, steady, dynamic compaction wave in granular HMX ($\lambda \equiv 0$) are given in Fig. 2 for the piston speed $u_p = 85.6$ m/s. The numerical solution technique used to solve the model equations is discussed in Section 4 of this report. Here, the compaction wave is shown propagating to the right at speed $D = 297.5$ m/s. A continuous, dispersed wave structure is predicted due to compaction induced mechanical dissipation. Similar low speed, dispersed structures have been experimentally observed [16, 21] and predicted by detailed meso-scale numerical simulations [17] for granular HMX. Smooth increases from their initial values are predicted for all quantities through the compaction zone. The solid volume fraction increases from its initial free pour value of $\phi_0 = 0.655$ to a final equilibrium compacted value of $\phi = 0.92$. The velocity increases from zero to u_p as required by the rear

5

boundary condition at the piston surface. The initially unstressed granular material reaches an equilibrium stress of $P_s = 34.5$ MPa in the compacted state. Importantly, the bulk temperature rise associated with the compaction process is only about $\Delta T = 2.4$ K which is much too low to initiate chemical reaction. Further, the bulk temperature rise for a piston speed of 400 m/s is only approximately 50 K. As such, combustion models that are based on bulk temperature are too insensitive to accurately predict the onset of self-sustained combustion for varying impact conditions. This issue motivates the need to develop rational energy localization models. It is shown in Ref. [9] that predictions of the bulk compaction model for equilibrium end states and compaction wave speeds agree well with experimental data for a wide range of piston speeds.

3.2 Energy Localization Model

In this subsection we describe a thermal energy localization model that is consistent with the bulk model. The localization model consists of 1) a model for the evolution of meso-scale structure, 2) a strategy for localizing bulk dissipated energy at the meso-scale, and 3) a model for predicting the meso-scale response.

3.2.1 Meso-Scale Structure

The meso-scale structure of granular HMX, and PBXs containing HMX and binder, consists of a broad distribution of grain sizes and shapes packed in complex arrangements. Experiments indicate that substantial changes in the meso-scale structure occur as the material is mechanically loaded [4, 19]. These changes are in large part due to the brittle nature of HMX that readily fractures when compressed; grain/binder deconsolidation is also observed in PBXs. A detailed model for the evolution of grain size distribution that accounts for grain fracture can be formulated using integral techniques [8], but the models are complex, computationally expensive to solve, and beyond the scope of this study. For now, we ignore grain fracture and track the evolution of grain number density $n(x, t)$ by

$$\frac{\partial n}{\partial t} + \frac{\partial}{\partial x}(nu) = 0. \tag{7}$$

Fracture can be accounted for, within the context of a size distribution function, by supplying a forcing term $\int_0^\infty \dot{F} dm$ in Eq. (7), where $\dot{F}(m, x, t)$ is the volumetric fracture rate per unit grain mass that must satisfy $\int_0^\infty m\dot{F} dm = 0$ for mass conservation; this topic will be the focus of future work. We additionally assume that the grains are incompressible and of uniform size and spherical shape; they can be characterized by their constant radii R. Grain number density is related to solid volume fraction and grain size by $n = \phi/(4/3\pi R^3)$. We do not give a detailed description of the grain packing arrangement, but specify the average number of intergranular contact points (surfaces) per grain, γ. As an illustration, a face centered cubic (FCC) arrangement of uniform size spherical grains has $\gamma = 12$, whereas a simple cubic (SC) arrangement has $\gamma = 6$. Though a real granular material will not have such an ordered arrangement, it is reasonable to assume $1 \le \gamma \le 16$. In summary, the meso-scale structure is characterized in this study by the variable ϕ and the constant parameters R and γ.

3.2.2 Localization Strategy

An appropriate energy localization strategy should include information based on the dissipative mechanics occurring at the material meso-scale. Applied bulk loads are transmitted at the meso-scale by intergranular contact. Experiments [20] and numerical simulations [17] indicate that the

6

Property	Value
E, Young's Modulus	24.0 GPa
Y, Yield Strength	0.37 GPa
ν, Poisson's Ratio	0.2
ρ_s, Density	1903.0 kg/m^3
c_v, Specific Heat	1.5 kJ/kg/K
k, Thermal Conductivity	0.502 W/m/K

Table 1: Material properties for HMX.

bulk load is not uniformly transmitted through the meso-structure, but is preferentially transmitted along certain paths that form stress chains; grains not involved in these chains remain mostly unstressed and inactive. It is reasonable then to expect that grain size, shape, and packing arrangement may have a large effect on the meso-scale stress state. The stress state will also depend on the magnitude of the applied load, and possibly the loading rate. For weak loads, the meso-structural response will mostly involve localized elastic deformation and friction near active intergranular contact points (surfaces). In this case, the elastic stress field in the vicinity of the contact surface is approximated by classical Hertz contact theory [13]. The onset of plastic deformation will occur within the grain, near the contact surface, at the location where the principal shear stress, τ, first equals the material yield strength, Y. An expression for τ based on the Hertz solution is given by

$$\tau = \frac{1}{2}P_c \left| (1+\nu)\left[1 - \left(\frac{z}{a}\right)\tan^{-1}\left(\frac{a}{z}\right)\right] - \frac{3}{2}\left[1 + \left(\frac{z}{a}\right)^2\right]^{-1} \right|, \tag{8}$$

where

$$a = \frac{\pi R^* P_c}{2E^*}, \tag{9}$$

and

$$R^* = \frac{R}{2}, \qquad E^* = \frac{E}{2(1-\nu^2)}.$$

Here, E is Young's modulus, ν is Poisson's ratio, P_c is the stress at the contact center, and z is distance into the grain normal to the planar, circular contact surface of radius a as shown in Fig. 3(a). We have assumed that contact occurs between spheres of equal size. For axi-symmetric contact, the onset of plastic deformation occurs when $P_c = 1.6Y$, which is based on von Mises' yield criterion. Both the maximum shear stress and its location within the grain at the onset of plastic deformation can be determined from Eq. (8). Using the material properties for HMX listed in Table 1, the onset of plastic deformation for a grain size of $R = 25$ μm will occur for $P_c = 0.59$ GPa at a depth $z = 0.45a = 0.93$ μm corresponding to $(\tau)_{\max} = 0.33P_c = 0.2$ GPa. Continued loading will cause the volume of plastically deformed material to increase resulting in plastic heating. Grain fracture and intergranular friction may also be significant, particularly at elevated loads. Bulk dissipated mechanical energy is the integrated effect of these meso-scale dissipative processes.

A phenomenological localization model can be developed based on the foregoing discussion. In so doing, we will make several simplifications and explore their consequences. Because both plastic deformation and friction occur in the neighborhood of intergranular contact points (surfaces), we will track solid regions surrounding these points within which bulk dissipated mechanical energy will be thermalized; these regions will be referred to as energy localization centers. The number of

localization centers per unit volume, $n_c(x,t)$, is related to the number of contact points per grain and grain number density by $n_c = \frac{1}{2}\gamma n$; the prefactor $1/2$ is introduced because each localization center involves contact between two grains. The localization centers are evenly distributed and individually surrounded by solid spheres of radii r_o, as shown in Fig. 3, where $r_o = R(\frac{1}{2}\gamma)^{\frac{1}{3}}$. The above expression for n_c can be combined with this expression for r_o to obtain $n_c = \phi/(\frac{4}{3}\pi r_o^3)$; thus, all solid mass is encompassed by the localization spheres. For an incompressible solid, as assumed in this study (i.e., $R = $ constant), r_o is constant for a given value of γ. Because grain contact surfaces in real materials would not be evenly distributed as assumed here due to stress chain formation and grain size variations, bulk thermal energy would be localized at a fewer number of closely packed localization sites; there may also exist significant thermal interaction between these sites. The present model can indirectly account for increased localization by reducing the value of γ, but does not account for asymmetrical thermal interaction between sites as discussed in the following subsection. We note, however, that a comparison of ignition predictions with experimental data for HMX suggests that the onset of sustained bulk combustion may be reasonably insensitive to the spatial distribution of localization sites. Nonetheless, the model can be generalized in the future to more accurately reflect these features.

Thermal energy will be deposited over a volume of radius $r_c(x,t) \leq r_o$ which defines the localization center. The initial value for r_c is taken as the radius of the intergranular contact surface, a, at the onset of plastic deformation within the grain. This volume is close to the elliptical volume defined by a and the distance from the contact surface at which plastic deformation first occurs, $z = 0.45a$. Thus, we have from Eq. (9) that

$$r_c(x,0) = \frac{\pi R^* P_c}{2E^*}, \tag{10}$$

where $P_c = 1.6Y$. This assumption is reasonable in that prior to the onset of plastic deformation most dissipated energy will be due to intergranular friction and will, thus, be localized near the contact surface within the region $r < r_c(x,0)$. It is noted that the initial localization volume decreases with grain size. To obtain an expression for the evolution of r_c due to material compaction, we assume that the material is perfectly plastic and is in an uncontained mode of plastic deformation; as such, details of the transitional range of loading associated with purely elastic, elastic-plastic, and fully plastic flow are not modeled. The plastic flow stress is taken to be $P_Y = 3.0Y$ [13]. This expression for flow stress has also been used to describe the quasi-static compaction behavior of
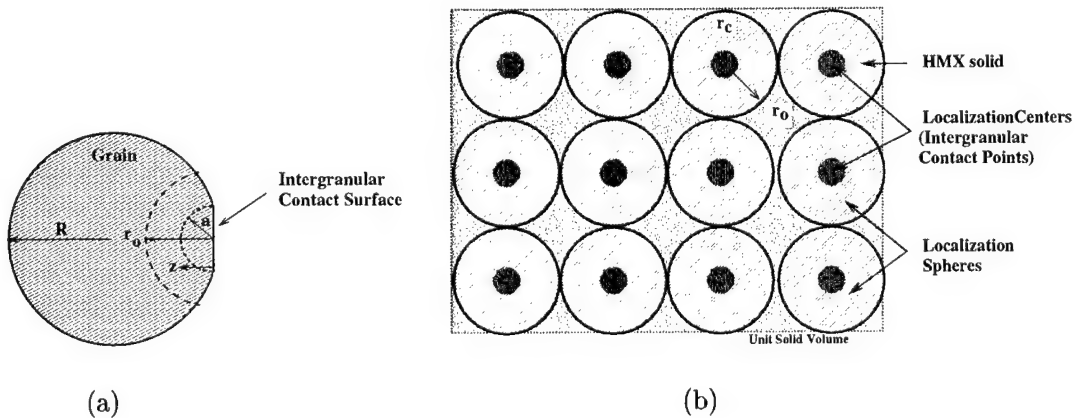

Figure 3: Schematic of the thermal energy localization strategy.

8

ball powder [11]. We equate the volumetric rate of work done by the plastic flow stress to the bulk volumetric dissipated energy given by Eq. (5):

$$n_c P_Y \frac{dV_c}{dt} = \rho_s \phi \frac{de_s}{dt}, \tag{11}$$

where $V_c = \frac{4}{3}\pi r_c^3$ is the localization (plastic) volume for a single sphere. An expression for the evolution of r_c is thus given by

$$\frac{dr_c}{dt} = \frac{\rho_s \phi}{4\pi r_c^2 n_c P_Y} \frac{de_s}{dt}, \tag{12}$$

where $P_Y = 3.0Y$. Though we have assumed that all bulk dissipated energy is the result of plastic deformation, the bulk dissipated energy can be easily partitioned into both frictional and plastic components; this would involve minimal modification of the model. The model sensitivity to variations in both the initial localization volume and the plastic flow stress is addressed in Subsection 4.3.

3.2.3   Meso-Scale Response

A model for the meso-scale response to localized heating will now be described. The approach is similar to the modified Frank-Kamenetskii thermal explosion theory of Foster, et al [6]. To this end, we track the time-dependent, radial evolution of thermal energy and chemical reaction progress of HMX contained within a single localization sphere subject to thermal energy deposition based on the strategy of Subsection 3.2.2. Evolution equations for thermal energy and reaction progress are given by the following, respectively:

$$\rho_s c_v \frac{d\hat{T}}{dt} = \frac{k}{r^2} \frac{\partial}{\partial r} \left(r^2 \frac{\partial \hat{T}}{\partial r} \right) + z \left(1 - \hat{\lambda} \right) \exp\left(-\frac{T_a}{\hat{T}} \right) q + \hat{S}, \tag{13}$$

$$\frac{d\hat{\lambda}}{dt} = z \left(1 - \hat{\lambda} \right) \exp\left(-\frac{T_a}{\hat{T}} \right). \tag{14}$$

Here, r is radial position within the localization sphere and $d/dt = \partial/\partial t + u\partial/\partial x$ is the convective derivative. It is necessary to include the convective derivative because the grains, and thus the localization spheres, locally propagate at the bulk velocity u. Variables labeled with a "hat" ($\hat{\bullet}$) are associated with the localization sphere and vary not only with x and t but also with r; they include solid temperature, $\hat{T}(x, r, t)$, reaction progress, $\hat{\lambda}(x, r, t)$ ($0 \le \hat{\lambda} \le 1$, where $\hat{\lambda} = 1$ is complete reaction), and volumetric thermal energy deposition rate $\hat{S}(x, r, t)$. The meso-scale and bulk models will be coupled through the energy source term $\hat{S}$. Constant parameters contained in Eqs. (13) and (14), and not yet defined, are thermal conductivity, k, Arrhenius prefactor, z, and activation temperature, T_a. Equation (13) is consistent with the caloric equation of state $\hat{e}_s = c_v \hat{T} - \hat{\lambda} q$. Equation (14) models a one-step, irreversible chemical reaction having Arrhenius kinetics. Values for the thermal and chemical parameters for HMX are given in Tables 1 and 2, respectively.

To maintain consistency between the meso-scale and bulk models, we require that the evolution of mass, linear momentum, and thermal energy at the meso-scale locally equals that given by the bulk model. It can be easily shown that the mass constraint is identically satisfied based on the expression for r_o given in Subsection 3.2.2. Also, because we are primarily interested in the meso-scale thermal energy response, we have assumed that all grains move at the local bulk velocity;

9

Property	Value
z, Arrhenius Prefactor	5.00×10^{19} s^{-1}
q, Specific Heat of Reaction	5.95×10^6 J/kg
T_a, Activation Temperature	2.65×10^4 K

Table 2: Chemical properties for HMX.

consequently, the linear momentum constraint is trivially satisfied. It remains to satisfy the thermal energy constraint given by

$$\frac{d}{dt}\left(\int \rho_s \phi e_s\right) dx = \frac{d}{dt}\left(\int \rho_s n_c \ 4\pi \int_0^{r_o} r^2 \hat{e}_s \ dr dx\right). \tag{15}$$

The left hand side of this equation is the evolution of bulk thermal energy for a volume element of arbitrary length in the x-direction, where $e_s = c_v T - \lambda q$ is the bulk specific internal energy. The right hand side of this equation is the evolution of integrated thermal energy at the meso-scale. Using the relation $n_c = \phi/(\frac{4}{3}\pi r_o^3)$ in Eq. (15) gives by inspection

$$e_s(x,t) = \frac{3}{r_o^3} \int_0^{r_o} r^2 \hat{e}_s(x,r,t) \ dr; \tag{16}$$

thus, for an incompressible solid, the bulk internal energy is the volumetric average of the energy contained within a localization sphere. Likewise, the following relations for the bulk temperature and reaction progress variable can be obtained from Eq. (16) using the expressions for e_s and $\hat{e}_s$:

$$T(x,t) = \frac{3}{r_o^3} \int_0^{r_o} r^2 \hat{T}(x,r,t) \ dr, \tag{17}$$

$$\lambda(x,t) = \frac{3}{r_o^3} \int_0^{r_o} r^2 \hat{\lambda}(x,r,t) \ dr. \tag{18}$$

The expression for $\hat{S}(x,r,t)$ must be chosen so that Eq. (16) is identically satisfied. To this end, we first take the convective derivative of Eq. (16), with r_o constant, to obtain

$$\frac{de_s}{dt}(x,t) = \frac{3}{r_o^3} \int_0^{r_o} r^2 \frac{d\hat{e}_s}{dt}(x,r,t) \ dr. \tag{19}$$

Next, the expression for $\hat{e}_s$ is differentiated and the result used to replace the derivative $d\hat{e}_s/dt$ in Eq. (19) in favor of the derivatives $d\hat{T}/dt$ and $d\hat{\lambda}/dt$, expressions for which are given by Eqs. (13) and (14), respectively. The resulting thermal conduction term vanishes when integrated due to zero heat flux conditions applied at the boundaries of the energy localization sphere [i.e., $\partial \hat{T}/\partial r(x,0,t) = \partial \hat{T}/\partial r(x,r_o,t) = 0$]. The zero heat flux at r_o implies symmetry between the uniformly spaced localization spheres; future work will relax this condition to allow for asymmetrical thermal interaction between spheres. Equation (19) then reduces to

$$\frac{de_s}{dt}(x,t) = \frac{3}{r_o^3} \int_0^{r_o} r^2 \frac{\hat{S}(x,r,t)}{\rho_s} \ dr. \tag{20}$$

This equation must be satisfied by our choice of $\hat{S}$. The thermal energy localization strategy specifies that bulk dissipated energy is deposited within localization centers defined by $r \leq r_c$, where the evolution of r_c is given by Eq. (12). Therefore, we take

$$\hat{S}(x,r,t) = \begin{cases} \left[\dfrac{r_o}{r_c(x,t)}\right]^3 \rho_s \dfrac{de_s}{dt}(x,t) & \text{for } 0 \leq r \leq r_c(x,t) \\[4mm] 0 & \text{for } r_c(x,t) < r \leq r_o \end{cases} \tag{21}$$

It is seen that for $\hat{S}$ to remain bounded as $r_c \to 0$ requires that $d\hat{e}_s/dt$ rapidly vanish in this limit. While it is not formally proven that this condition exists, we note that the singularity posed no numerical difficulties in this study.

In summary, the energy localization model is given by Eqs. (7), (12), (13), and (14), where $\hat{S}$ is given by Eq. (21), $n_c = \frac{1}{2}\gamma n$, and $r_o = R(\frac{1}{2}\gamma)^{\frac{1}{3}}$. This meso-scale model is coupled to the bulk model through the thermal energy equation, given by Eq. (5), and the solid volume fraction. The composite model is mathematically closed and can be solved, in principle, when suitable initial and boundary conditions are supplied.

4 Results

As an illustration of the model, we perform an analysis of localized heating and ignition of granular HMX by steady compaction waves resulting from constant speed piston impact. The focus of this analysis is on low speed impact associated with weak initiation of DDT in heavily confined tubes of granular HMX [4, 16]. The analysis is similar to that given by Gonthier and Son [10].

The model equations are solved in a compaction wave-attached frame defined by the transformation $\xi = x - Dt$ and $v = u - D$, where D is the steady speed of a right propagating wave. Because the model is frame invariant, the governing equations in the wave frame have the same form as those given in Section 3 with x replaced by ξ and u replaced by v. The analysis is restricted to compaction waves propagating with speeds much less than the ambient solid acoustic speed ($D \ll 3000$ m/s) due to the incompressibility assumption. We also assume that $P_c\tilde{\mu}/\mu_c \ll 1$, where P_c is a characteristic compaction stress; thus, Eq. (3) is replaced by the equilibrium condition $\tilde{\phi} = f(\phi)$. We take $\mu_c = 100$ kg/(s m). For brevity, the constitutive relations for both $f(\phi)$ and $\beta(\phi, \tilde{\phi})$ are not given here, but can be found in Ref. [9]. With these assumptions, the steady problem can be reduced to the following initial-boundary value problem (details of the mathematical reductions are omitted):

$$\frac{d\phi}{d\xi} = \frac{\phi(1-\phi)}{v\mu_c}\left(P_s - \beta\right), \tag{22}$$

$$\frac{\partial \hat{T}}{\partial \xi} = \frac{\alpha}{vr^2}\frac{\partial}{\partial r}\left(r^2 \frac{\partial \hat{T}}{\partial r}\right) + \frac{z}{\rho_s c_v v}\left(1 - \hat{\lambda}\right)\exp\left(-\frac{T_a}{\hat{T}}\right)q + \frac{\hat{S}}{\rho_s c_v v}, \tag{23}$$

$$\frac{\partial \hat{\lambda}}{\partial \xi} = \frac{z}{v}\left(1 - \hat{\lambda}\right)\exp\left(-\frac{T_a}{\hat{T}}\right), \tag{24}$$

$$\frac{dr_c}{d\xi} = \frac{(P_s - \beta) + f'\beta}{4\pi r_c^2 n_c P_Y}\frac{d\phi}{d\xi}, \tag{25}$$

where $\alpha = k/(\rho_s c_v)$ and $f' = df/d\phi$. We have substituted Eq. (5) into Eq. (12), and used the relation $\tilde{\phi} = f$, to obtain Eq. (25). The bulk mechanical response of the granular material is

11

given solely by the solution of Eq. (22) as the variables v, P, β, and $\tilde{\phi}$ depend only on ϕ. Bulk temperature and reaction progress are related to the meso-scale response by Eqs. (17) and (18), respectively. Initial conditions for the unstressed granular solid are $\phi(0) = 0.655$, $\hat{T}(0, r) = 300$ K, $\hat{\lambda}(0, r) = 0$, and $r_c(0) = 1.6\pi R^* Y/(2E^*)$. Boundary conditions for the meso-scale model are $\partial \hat{T}/\partial r(\xi, 0) = \partial \hat{T}/\partial r(\xi, r_o) = 0$. The system of partial differential equations (PDEs) is numerically solved by a Method of Lines technique using an implicit, stiff ordinary differential equation (ODE) solver contained in the package LSODE. To this end, the radial coordinate of the localization sphere is discretized into 100 evenly spaced nodes and the radial derivative in Eq. (23) is approximated by a second-order accurate centered finite-difference relation. The numerical method was validated against analytical solutions for compaction end states and simple heat conduction problems.

The bulk compaction problem has already been discussed in Subsection 3.1, and is discussed in detail in Ref. [9]; thus, the predicted meso-scale response is the focus of this section. We first give predictions for the localized heating of inert HMX (i.e., for $\hat{\lambda} \equiv 0$) for $u_p = 85.6$ m/s, and then consider reactive HMX for this same value of u_p. This piston speed is chosen because it is close to that needed for the predicted onset of sustained combustion. The corresponding compaction wave speed is $D = 297.5$ m/s. The values $R = 25$ μm and $\gamma = 12$ are used as representative of lightly compacted granular HMX. Model sensitivity to variations in these and other parameters is demonstrated. The evolution of ϕ, u, and P within the compaction zone for both of these simulations are given in Fig. 2.

All numerical simulations performed in this study were solved on a Dell OptiPlex GX400 workstation having a single INTEL Pentium IV, 1.3 GHz processor. The average computational run time for a single simulation was approximately 5 seconds.

4.1 Inert Compaction

Figure 4 gives predictions of the energy localization model for heating within the compaction zone of inert HMX. Grain number density smoothly increases from its initial value of $n = 1.11 \times 10^7$ grains/cm^3 to an approximate equilibrium value of 1.41×10^7 grains/cm^3 through the wave as the material is compacted. The equilibrium value for the number of energy localization sites is $n_c = \frac{1}{2}\gamma n = 8.46 \times 10^7$ sites/cm^3. Compaction induces mechanical energy dissipation within material contained by localization centers that individually surround grain contact points. The spherical volume of material contained within a localization center, characterized by its radius r_c, increases from its initial value of $r_c = 0.93$ μm to a final value of 2.55 μm. As mentioned, this volume increase is interpreted as the uncontained spreading of plastically deformed material due to intergranular contact. The outer radius of the localization sphere remains constant at $r_o = 13.76$ μm because the solid grains are assumed incompressible. A pulse-like volumetric heat deposition rate is predicted for the localization center, reaching the maximum value $\hat{S} = 0.52$ GW/cm^3 within the compaction zone where $\phi = 0.73$ at $\xi = -3.71$ mm. Though this rate is high, it is well below the characteristic heat generation rate of approximately $\hat{S}_d = \rho_s q D_d/L_d = 3.1 \times 10^4$ GW/cm^3 (for $D_d = 7000$ m/s and $L_d = 2.55$ μm) that would be associated with detonation of the solid HMX contained within the localization center. This heating gives rise to the temperature field of Fig. 4(e). The plot shows radial temperature profiles within a localization sphere though the compaction zone. A maximum temperature of 735.5 K is predicted at the center of the localization sphere at $\xi = -4.69$ mm; thus, the peak temperature within the compaction zone trails the peak energy deposition rate. The temperature rapidly decreases as the applied energy deposition rate vanishes. Though not shown here, the temperature field within the localization sphere will approach the

uniform bulk value of $T = 302.4$ K as $\xi \to -\infty$. This feature is a consequence of having energetically consistent localization and bulk models.

Inspection of Figs. 4(c) and (e) indicates that much of the applied thermal energy remains in the vicinity of the localization center through the compaction wave as there is little time for conduction into the cooler grain interior. This observation does not imply that thermal conduction is unimportant in the heating process. An estimate for the change in temperature of material contained in the localization center in the absence of thermal conduction is given by $\Delta T = \hat{\mathcal{S}}_{avg}\mathcal{T}/(\rho_s c_v)$, where $\hat{\mathcal{S}}_{avg}$ and $\mathcal{T}$ are the average applied energy deposition rate and grain residence time within the compaction zone, respectively. Taking $\hat{\mathcal{S}}_{avg} = 0.2$ GW/cm^3 and $\mathcal{T} = 19$ μs, which are characteristic of the predictions shown here, then $\Delta T = 1331$ K. Indeed, the same simulation performed with $\alpha = 0$ m^2/s predicts a temperature within the localization center that is in excess of 1400 K. We further determine the mass fraction of heated material, X, having temperature within intervals of approximately 10 K over the range $300 \leq \hat{T} \leq 750$ K; the result is shown in Fig. 4(f). Only a small fraction of the total mass is heated to elevated temperatures within the compaction zone, and this mass is rapidly cooled by thermal conduction as the energy deposition rate diminishes. An important question is whether the heated mass has sufficient thermal inertia to trigger the onset of sustained combustion. This question is answered in the following subsection.

We lastly remark that phase change, not accounted for by the model, will affect predicted temperatures. A relevant discussion is given by Menikoff and Kober [17]. While phase change would reduce predicted temperatures due to the latent heat of fusion, thermal energy localization in real materials will likely be more pronounced than predicted here due to stress chain formation. As such, these predictions are considered a reasonable *average* localization response. The inclusion of phase change will be addressed at a later time.

4.2   Reactive Compaction

Figure 5 gives predictions of the energy localization model for heating and chemical reaction within the compaction zone of HMX. Profiles for n, n_c, r_c, r_o, and $\hat{\mathcal{S}}$ are the same as those given in Fig. 4. The predicted variation through the compaction zone of the radial temperature profile within a localization sphere is shown in figure (a); the corresponding variation in local reaction progress is shown in (b). The temperature near the center of the sphere is sufficient to induce chemical reaction that locally goes to completion ($\hat{\lambda} = 1$). The reaction accelerates almost to the point of thermal explosion as indicated by the presence of a sharp temperature spike. However, thermal energy conduction from the reaction site into the grain interior freezes the reaction causing a rapid decrease in temperature. A peak temperature in excess of 1200 K is predicted prior to extinction of chemical reaction. The predicted evolution of hot-spot mass fraction is shown in figure (c). As before, only a small fraction of the total mass is heated to elevated temperatures, and its thermal inertia is insufficient to overcome thermal conduction losses and achieve sustained combustion.

The predicted variation in bulk temperature and reaction progress through the compaction zone are shown in Fig. 6. Because bulk temperature depends on the temperature field within a localization sphere by Eq. (17), the profile is not identical to that that given in Fig. 2(d) for the inert case. However, since chemical reaction is mostly confined to a very small volume of material near the sphere center, the equilibrium value of bulk temperature following compaction is also approximately $T = 302.4$ K.
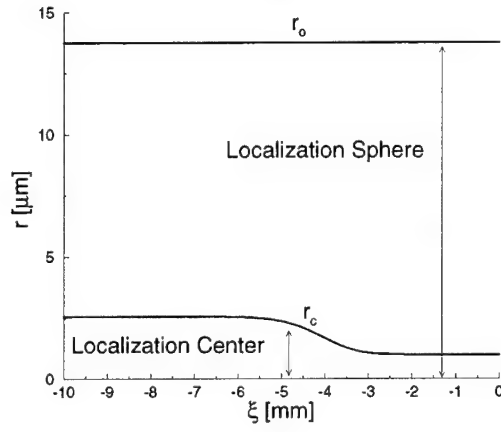
For this simulation, $u_p = 85.6$ m/s. Numerical experiments indicate that this piston speed is close to the thermal explosion threshold; the value $u_p = 85.7$ m/s results in a thermal explosion
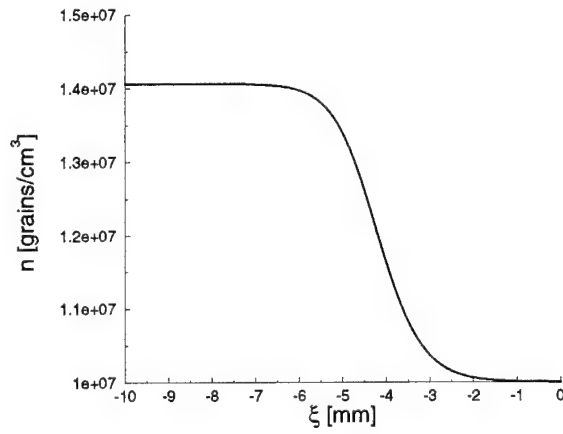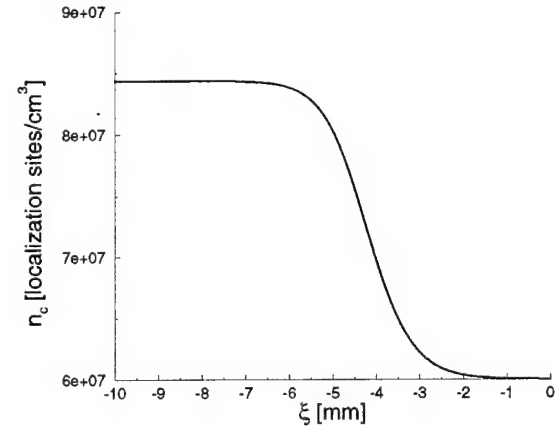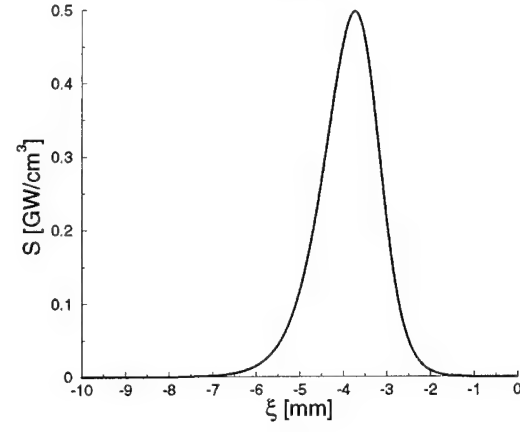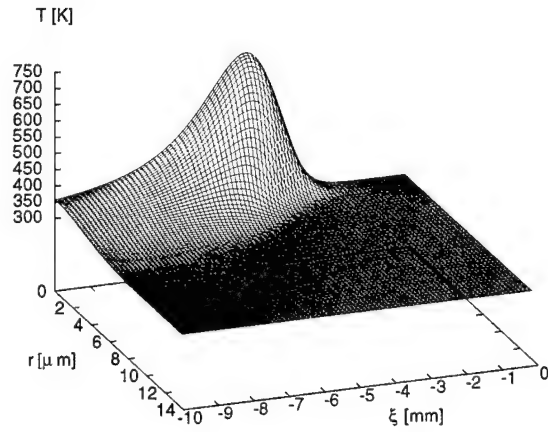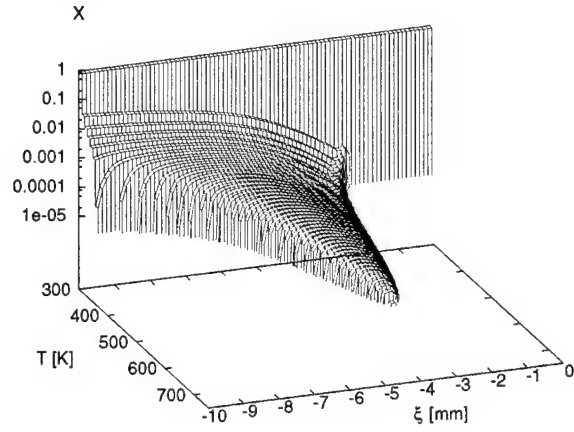
Figure 4: Predicted localized heating through the compaction zone for inert HMX ($u_p = 85.6$ m/s): (a) grain number density, (b) localization center number density, (c) localization center radius, (d) volumetric heating rate, (e) local temperature, and (f) hot-spot mass fraction.

14

marking the onset of sustained combustion of the material. This prediction agrees well with the results of confined DDT tube tests involving piston impact of granular HMX [16, 22]. These tests indicate that the explosion is first triggered for piston speeds approximately in the range $80 \leq u_p \leq 90$ m/s. Combustion is often observed for piston speeds slightly below this threshold, but transition to detonation does not occur.
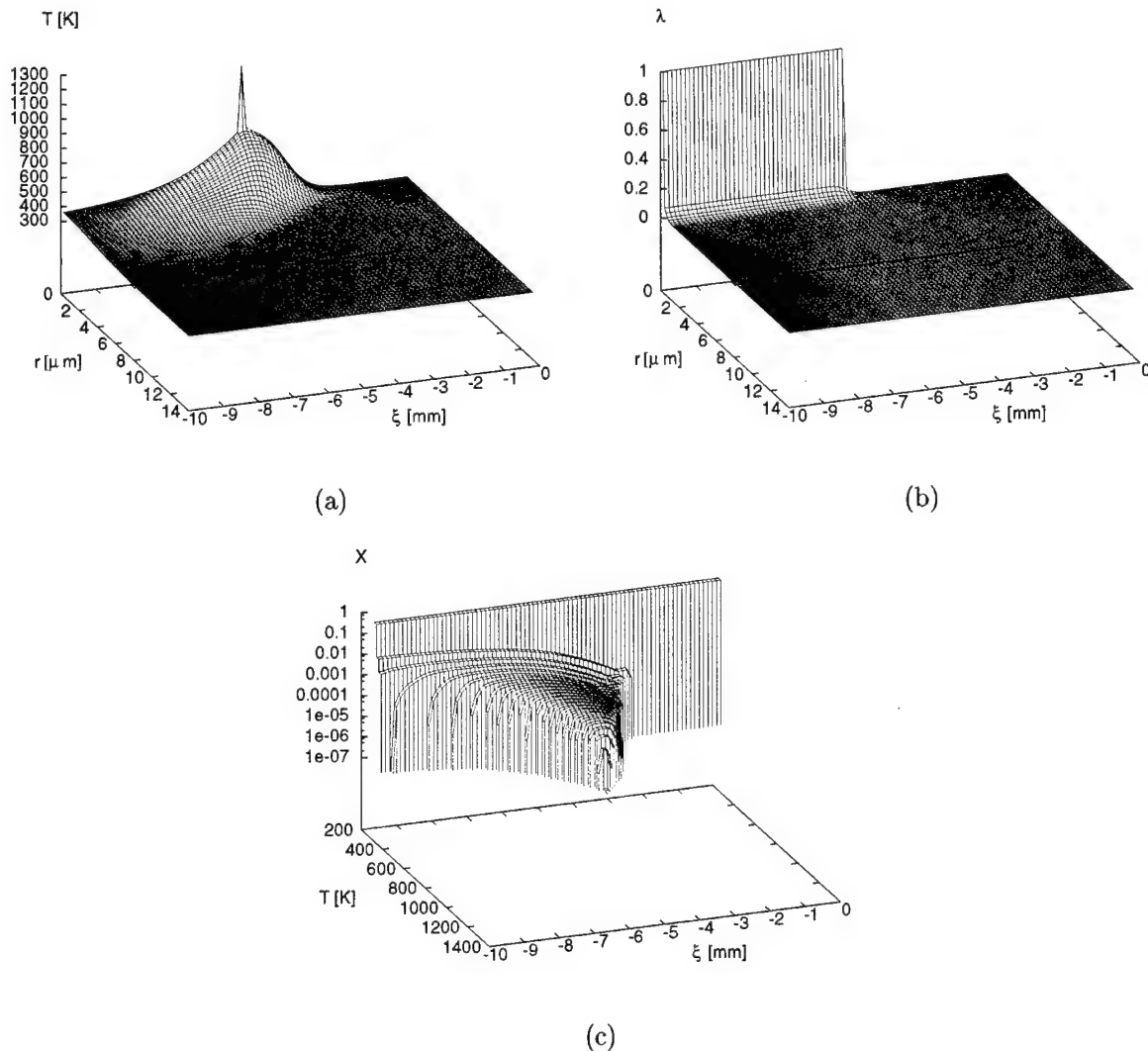

(a)

(b)

(c)

Figure 5: Predicted heating and reaction progress through the compaction zone for HMX ($u_p = 85.6$ m/s): (a) local temperature, (b) local reaction progress, and (c) hot-spot mass fraction.

4.3   Parametric Sensitivity

Numerical experiments were performed to determine the model sensitivity to variations in key energy localization parameters. To this end, parameter values used for the reactive compaction simulation were chosen as a baseline, and the values of γ, P_c/Y, and P_Y/Y were independently varied over physically significant ranges. The piston speed needed for sustained combustion (ther-
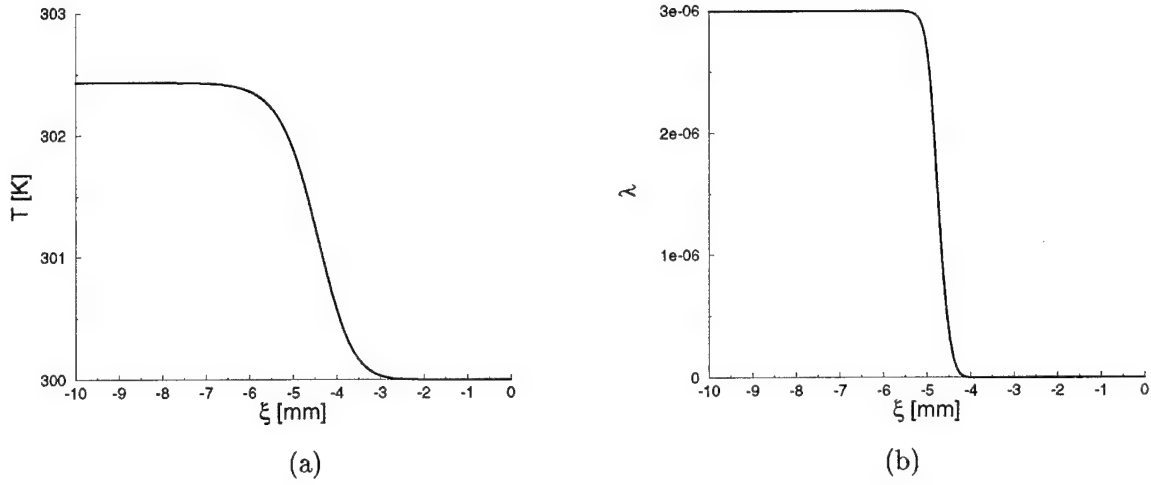
15

Figure 6: Predicted bulk (a) temperature and (b) reaction progress through the compaction zone for HMX ($u_p = 85.6$ m/s).

mal explosion) was determined for each case. Here, the value of γ determines the hot-spot density of the meso-structure. The ratio P_c/Y determines the initial radius of the localization center, $r_c(0)$, as seen from Eq. (10), and the ratio P_Y/Y determines the growth rate of r_c, given by Eq. (12). Thus, both of these ratios control the volume over which bulk dissipated energy is localized. Because grain size is an important, easily adjustable system parameter, its influence on the predicted onset of sustained combustion was also determined.

Results of the sensitivity analysis are summarized in Fig. 7. The value of γ was varied over the range $1 \leq \gamma \leq 14$; it is reasonable to expect that, on average, the number of contact points per grain lies within this range. The predicted threshold for sustained combustion increases with γ as bulk dissipated energy is distributed over a larger material volume. Values for P_c/Y and P_Y/Y were varied over the ranges $0.1 \leq P_c/Y \leq 3.0$ and $1.6 \leq P_Y/Y \leq 6.0$ which are typical of contact problems [13]. The sustained combustion threshold is predicted to increase with P_c/Y and decrease with P_Y/Y; these results are a consequence of bulk dissipated energy being localized over larger and smaller material volumes, respectively. Importantly, all of these predictions are near the experimentally observed explosion threshold for granular HMX. This result suggests that the localization strategy used in this study may be a viable approach to develop improved ignition models for heterogeneous reactive solids.

Lastly, the influence of grain size on the predicted combustion threshold is shown in Fig. 7(d). Here, it is seen that the piston speed for sustained combustion rapidly increases as grain size decreases. A value of $u_p = 384.2$ m/s is needed to trigger sustained combustion for a material composed of $R = 2.5$ μm size grains. This result agrees with experimental observations which show the same trend. Further, the necessary piston speed decreases only slightly for grains having approximately $R > 30$ μm.

5 Conclusions

This report summarized a model and analysis of mechanically induced hot-spot formation and ignition of granular HMX that is associated with weak initiation of DDT. To this end, a bulk
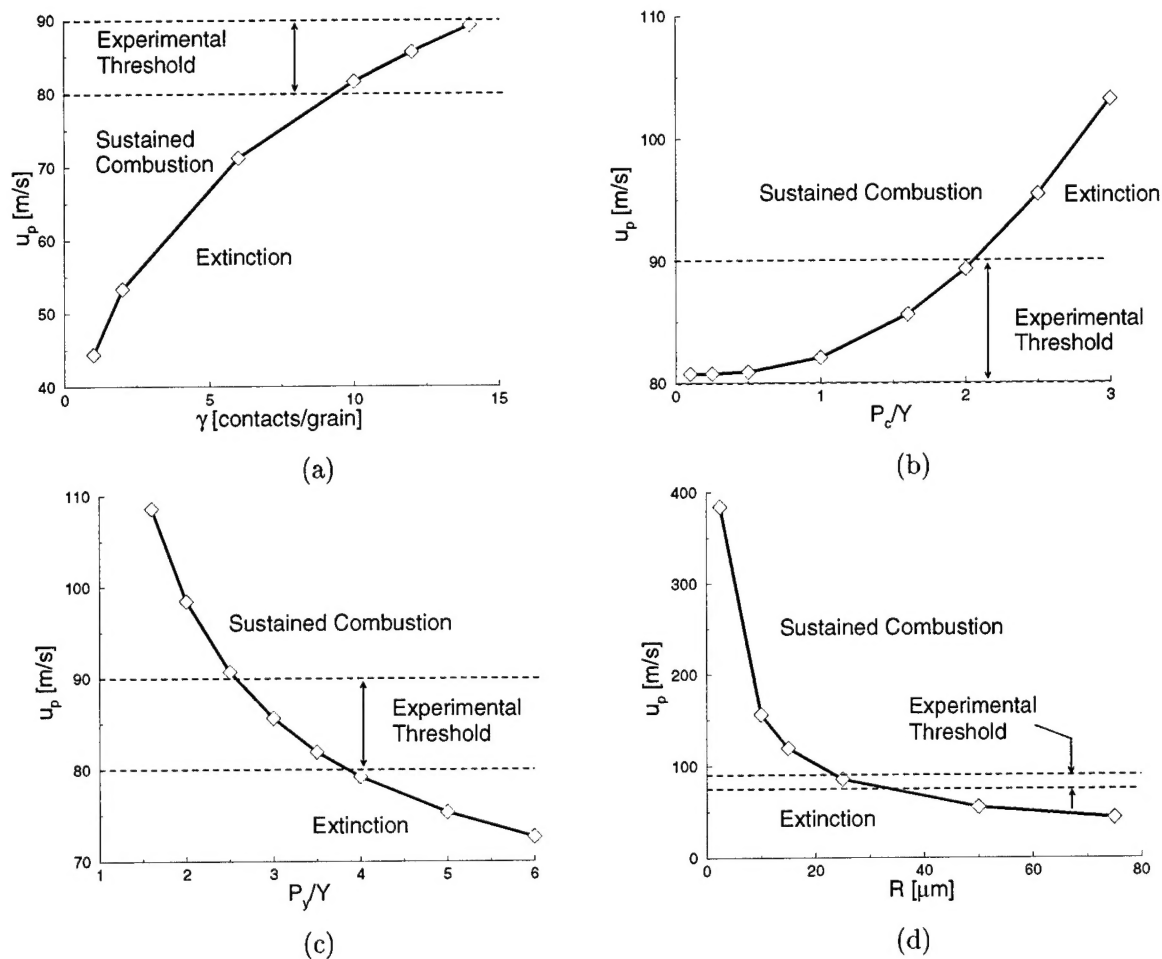
16

Figure 7: Sensitivity analysis results: (a) contacts/grain, γ; (b) initial localization center radius, characterized by P_c/Y; (c) localization center radius growth rate, characterized by P_Y/Y; and (d) grain size, R.

compaction model was coupled with a meso-scale model that tracked the evolution of hot-spots within the material meso-structure. Importantly, the interplay between localized energy deposition, thermal conduction, and chemical reaction at the grain scale was resolved. The deposition of bulk dissipated mechanical energy in the vicinity of intergranular contact points was guided by basic principles of contact mechanics. The bulk and meso-scale models were coupled in an energetically consistent manner which preserved the integrity of the experimentally correlated bulk predictions.

Localized heating predictions indicate that temperatures sufficient to induce chemical reaction can result from weak piston impact. Temperatures near 700 K were predicted for piston speeds near 86 m/s, the value needed for the onset of sustained combustion. This result agrees well with experimentally determined explosion thresholds for granular HMX. Also, thermal conduction was shown to have a significant influence on the ignition process; in the absence of thermal conduction, excessively high temperatures were predicted near intergranular contact points. The inclusion of thermal conduction is, thus, believed essential for accurately describing the weak initiation of DDT. Results of this study suggest that mechanically induced ignition can be accurately predicted

17

if important meso-scale features responsible for hot-spot formation are resolved.

Predictions showing the model response to variations in key energy localization parameters indicate that it is reasonably insensitive to the localization strategy. Because the model already gives results that agree well with experiments, it is possible that very good predictability can be obtained by including a more detailed description of the localization process including compressibility, stress chain formation, phase change, and grain fracture. Such a description would greatly increase model complexity and thus necessitate the use of modern computational tools for its accurate, efficient, and timely solution. Information provided by meso-scale experiments and numerical simulations can be used to guide the development of improved energy localization strategies.

Acknowledgments

References

[1] Baer, M. R., and Nunziato, J. W., "A Two-Phase Mixture Theory for the Deflagration-to-Detonation Transition in Reactive Granular Materials," *International Journal of Multiphase Flow*, Vol. 12, 1986, pp. 861-889.

[2] Baer, M. R., "Numerical Studies of Dynamic Compaction of Inert and Energetic Granular Materials," *Journal of Applied Mechanics*, Vol. 55, 1988, pp. 36-43.

[3] Boddington, T., "The Growth and Decay of Hot-Spots and the Relation Between Structure and Stability," Proceedings of the Ninth (International) Symposium on Combustion, Ithaca, New York, 1962, Academic Press, New York, 1963, pp. 287-293.

[4] Burnside, N. J., Son, S. F., and Asay, B. W, "Thick Walled DDT Tube Experiments," Presented at the 1996 JANAF PSHS Meeting, Naval Postgraduate School, Monterey, California, Nov. 4-8, 1996.

[5] Coyne, P. J., Elban, W. L., and Chiarito, M. A., "The Strain Rate Behavior of Coarse HMX Porous Bed Compaction," Proceedings of the Eighth (International) Detonation Symposium, 1989, pp. 645-657.

[6] Foster, J. C., Jr., Christopher, F. R., Wilson, L. L., and Osborn, J., "Mechanical Ignition of Combustion in Condensed Phase High Explosives," *Shock Compression of Condensed Matter*, American Institute of Physics, 1997, pp. 389-392.

[7] Friedman, M. H., "A Correlation of Impact Sensitivities by Means of the Hot-Spot Model," Proceedings of the Ninth (International) Symposium on Combustion, Ithaca, New York, 1962, Academic Press, New York, 1963, pp. 294-302.

[8] Gonthier, K. A., "A Model for the Morphological Evolution of Compacted Granular Materials," unpublished notes.

[9] Gonthier, K. A., Menikoff, R., Son, S. F., and Asay, B. W., "Modeling Compaction Induced Energy Dissipation of Granular HMX," Proceedings of the Eleventh (International) Detonation Symposium, 1998, pp. 153-161.

[10] Gonthier, K. A., and Son, S. F., "Modeling Compaction Induced Energy Localization in Granular HMX," *Shock Compression of Condensed Matter*, American Institute of Physics, 1999, pp. 393-396.

[11] Jacobs, S. J., Sandusky, H. W., and Elban, W. L., "Quasi-Static Compaction of Porous Propellant Beds. I. Modeling Ball Powder Experiments with Deformed Spheres in a Regular Lattice," *Powder Technology*, Vol. 89, 1996, pp. 209-217.

[12] Johnson, J. N., Tang, P. K., and Forest, C. A., "Shock-Wave Initiation of Heterogeneous Reactive Solids," *Journal of Applied Physics*, Vol. 57, No. 9, 1985, pp. 4323-4334.

[13] Johnson, K. L., *Contact Mechanics*, Cambridge University Press, New York, 1985.

[14] Kang, J., Butler, P. B., and Baer, M. R., "A Thermochemical Analysis of Hot Spot Formation in Condensed-Phase, Energetic Materials," *Combustion and Flame*, Vol. 89, 1992, pp. 117-139.

[15] Massoni, J., Saurel, R., Baudin, G., and Demol, G., "A Mechanistic Model for Shock Initiation of Solid Explosives," *Physics of Fluids*, Vol. 11, No. 3, 1999, pp. 710-736.

[16] McAfee, J. M., Asay, B. W., Campbell, W., and Ramsay, J. B., "Deflagration to Detonation Transition in Granular HMX," Proceedings of the Ninth (International) Detonation Symposium, 1989, pp. 265-278.

[17] Menikoff, R., and Kober, E., "Compaction Waves in Granular HMX," Los Alamos Report, LA-13546-MS, Los Alamos National Laboratory, Los Alamos, New Mexico, 1999.

[18] Powers, J. M., Stewart, D. S., and Krier, H., "Analysis of Steady Compaction Waves in Porous Materials," *Journal of Applied Mechanics*, Vol. 56, 1989, pp. 15-24.

[19] Roessig, K. M., Foster, J. C., Jr., and Wilson, L. L., "High Strain Rate Behavior of Plastic Bonded Explosives," presented at the International Workshop on New Models and Predictive Methods for Shock Wave/Dynamic Processes in Energetic Materials and Related Solids, University of Maryland, College Park, Maryland, July 4-9, 1999.

[20] Roessig, K. M., and Foster, J. C., Jr., "Experimental Simulations of Dynamic Stress Bridging in Plastic Bonded Explosives," Proceedings of the 2001 APS Conference on the Shock Compression of Condensed Matter, Atlanta, Georgia, 2001.

[21] Sandusky, H. W., and Liddiard, T. P., "Dynamic Compaction of Porous Beds," Naval Surface Warfare Center Technical Report, No. 83-246, 1985.

[22] Son, S. F., and Burnside, N. J., private communication, 1998.

[23] Tarver, C. M., Chidester, S. K., and Nichols, A. L., III, "Critical Conditions for Impact- and Shock-Induced Hot Spots in Solid Explosives," *Journal of Physical Chemistry*, Vol. 100, 1996, pp. 5794-5799.